

1 **Unsteady Ekman–Stokes dynamics: implications for**
2 **surface-wave induced drift of floating marine litter**

3 **C. Higgins^{1,2}, J. Vanneste², T.S. van den Bremer¹**

4 ¹Department of Engineering Science, University of Oxford, Oxford, OX1 3PJ, UK

5 ²School of Mathematics and Maxwell Institute for Mathematical Sciences, University of Edinburgh,
6 Edinburgh EH9 3FD, UK

7 **Key Points:**

- 8 • Marine litter studies include surface wave transport by Stokes drift but have ne-
9 glected wave-induced Eulerian-mean flows in the upper ocean.
10 • We present a model of the Eulerian-mean Ekman–Stokes response to time-varying
11 Stokes drift for use in marine litter transport models.
12 • Using buoy data we show the unsteady Ekman–Stokes flow significantly alters both
13 magnitude and direction of near-surface transport.

Corresponding author: Christopher Higgins, christopher.higgins@keble.ox.ac.uk

Abstract

We examine Stokes drift and wave-induced transport of floating marine litter on the surface of a rotating ocean with a turbulent mixed layer. Due to Coriolis–Stokes forcing and surface wave stress, a second-order Eulerian-mean flow forms, which must be added to the Stokes drift to obtain the correct Lagrangian velocity. We show that this wave-driven Eulerian-mean flow can be expressed as a convolution between the unsteady Stokes drift and an ‘Ekman–Stokes kernel’. Using this convolution we calculate the unsteady wave-driven contribution to particle transport. We report significant differences in both direction and magnitude of transport when the Eulerian-mean Ekman–Stokes velocity is included.

Plain Language Summary

In transport models for floating marine litter, surface wave effects are often included by simply superimposing their Stokes drift (the small net drift induced by waves) upon wind-driven flows and currents. However, due to Earth’s rotation and turbulent dissipation in the ocean’s surface mixed layer, the Stokes drift also drives additional Eulerian-mean flows. To obtain the correct transport velocity, the wave-induced Eulerian-mean flow must be added to the Stokes drift. We develop a model that enables estimation of this wave-induced Eulerian-mean flow from measurements or predictions of the wave field and apply our model to buoy data. Accounting for the Eulerian-mean flow significantly alters predictions of transport of floating marine litter.

1 Introduction

Floating marine debris, including plastic pollution, has rapidly become one of the most pressing environmental problems (Eriksen et al., 2014), particularly for marine ecosystems (Lavender Law, 2017). Although consensus exists about the longevity of plastic in the marine environment (Andrady, 2011) and the relatively large buoyancy of a significant share of plastic produced (Geyer et al., 2017), with both factors contributing to their long-distance transport, the total plastic budget of the world’s oceans is poorly understood. A significant mismatch exists between the estimated amount of land-generated plastic that enters coastal waters (5–12 million tonnes yr^{-1} , Jambeck et al. (2015)) and the estimated total amount of plastic floating at sea (less than 0.3 million tonnes, Cózar et al. (2014); Eriksen et al. (2014); van Sebille et al. (2015)). Similarly, the amount of plastics measured at sea over the last few decades (Lebreton et al., 2019; Ostle et al., 2019; Wilcox et al., 2020) has not kept pace with growth in global plastic production (Goldstein et al., 2012; Geyer et al., 2017). To understand this mismatch, an improved understanding of the physical processes governing the transport and dispersion is required (van Sebille et al., 2020). This letter focuses on one of these processes: surface waves.

As a particle undergoes its periodic motion beneath surface waves, it experiences a Lagrangian-mean velocity in the waves’ direction known as Stokes drift (Stokes, 1847). More generally, Stokes drift is the difference between the average Lagrangian flow velocity of a fluid parcel and the average Eulerian flow velocity of the fluid measured at a fixed spatial location (e.g. Bühler (2014); van den Bremer & Breivik (2017)). Surface gravity waves on the open ocean are mostly caused by winds. At any location and time, the wave field is a superposition of waves that have been generated by earlier winds at another location. Wave models, such as WAM and WaveWatch-III (Tolman, 2009), have been developed to predict wave fields and thus Stokes drift (Webb & Fox-Kemper, 2011; Breivik et al., 2014).

A recent and growing body of literature is examining the role of Stokes drift in the transport and dispersion of floating plastic pollution. Iwasaki et al. (2017) showed that in the Sea of Japan, Stokes drift pushed microplastics closer to the coast. Delandmeter

63 & van Sebille (2019) and Onink et al. (2019) report a similar result in Arctic regions.
 64 Dobler et al. (2019) demonstrated that Stokes drift fundamentally changes transport pat-
 65 terns in the South Indian Ocean by shifting the convergence regions to the west, caus-
 66 ing leakage into the South Atlantic rather than the South Pacific. Waves may also al-
 67 low particles to cross strong circumpolar winds and currents (Fraser et al., 2018).

68 Crucially, the above studies have simply superimposed the Stokes drift obtained
 69 from the local wave field onto the Eulerian current field obtained from ocean general cir-
 70 culation models or observations. In doing so, they have ignored the fact that the Eule-
 71 rian flow is itself modified by surface waves: on the rotating Earth, the Coriolis force as-
 72 sociated with the Stokes drift drives an Eulerian-mean current in the turbulent upper-
 73 ocean boundary layer (Ursell, 1950; Hasselmann, 1970; Xu & Bowen, 1994; Lewis & Belcher,
 74 2004), as noted in Onink et al. (2019). Together, the Stokes drift and this wave-induced
 75 Eulerian current form the Lagrangian velocity with which marine litter is transported.
 76 It is this wave-induced Eulerian current, which we call the Ekman–Stokes flow, that this
 77 letter examines.

78 We derive a model for computing the unsteady Eulerian-mean Ekman–Stokes re-
 79 sponse to a time-varying Stokes drift, taking into account the correct wave stress bound-
 80 ary condition and the Coriolis–Stokes forcing. We do so for the case of constant eddy
 81 viscosity in the turbulent upper-ocean layer and a quasi-monochromatic (or narrow-banded)
 82 wave field. The product of this letter is an Ekman–Stokes convolution kernel, which can
 83 readily be used to predict the wave-induced Eulerian-mean flow in the turbulent upper-
 84 ocean boundary layer and hence the Lagrangian transport of floating marine debris. This
 85 kernel is a low-computational-cost alternative to fully coupled general circulation and
 86 wave models, which include the effect of waves in both the Coriolis–Stokes forcing and
 87 the surface boundary condition (Breivik et al., 2015). Using sample wave field data from
 88 buoys, we show that accounting for the Eulerian-mean Ekman–Stokes response to a time-
 89 varying Stokes drift considerably alters the trajectories of drifting objects.

90 2 Unsteady Ekman–Stokes flow

We consider a homogeneous, incompressible ocean of constant depth d , described
 by horizontal coordinates x and y , and a vertical coordinate z measured upwards from
 the undisturbed water level. The governing equations are

$$\partial_t \mathbf{u} + \mathbf{u} \cdot \nabla \mathbf{u} + \mathbf{f} \times \mathbf{u} = -\nabla p + \nu \nabla^2 \mathbf{u}, \quad \nabla \cdot \mathbf{u} = 0, \quad (1a)$$

$$w|_{z=\eta} = \partial_t \eta + \mathbf{u}_H|_{z=\eta} \cdot \nabla_H \eta, \quad \hat{\mathbf{n}} \cdot \overleftrightarrow{\boldsymbol{\tau}} \cdot \hat{\mathbf{s}}|_{z=\eta} = 0, \quad (1b)$$

$$w|_{z=-d} = 0, \quad (1c)$$

91 where $z = \eta(x, y, t)$ denotes the free surface elevation, \mathbf{u} is the three-dimensional ve-
 92 locity vector, \mathbf{f} the Coriolis vector, $\mathbf{A}_H \equiv (A_x, A_y, 0)$ the horizontal component of any
 93 \mathbf{A} , and $\overleftrightarrow{\boldsymbol{\tau}}$ the stress tensor with components $\tau_{ij} = -(p - p_0)\delta_{ij} + \nu(\partial_i u_j + \partial_j u_i)$, with
 94 p_0 the atmospheric pressure and ν is the turbulent eddy viscosity, both taken constant.
 95 The unit vectors $\hat{\mathbf{n}}$ and $\hat{\mathbf{s}}$ are normal and tangential to the free surface respectively, so
 96 the dynamic boundary condition is a stress-free condition.

97 2.1 Wave-averaged mean-flow equations

98 We assume the wave steepness is small, $\alpha \equiv kA \ll 1$, where A is the peak wave
 99 amplitude of η and k the peak wavenumber, and solve (1) to $O(\alpha^2)$ using a Stokes ex-
 100 pansion $\mathbf{u} = \mathbf{u}_1 + \mathbf{u}_2 + \dots$, where the subscript denotes the order in α . We focus on
 101 deep-water waves ($kd \gg 1$).

102 Linear wave dynamics arises at $O(\alpha)$, where we ignore viscous effects, neglecting
 103 a thin vorticity boundary layer of thickness $\delta_\nu = \sqrt{2\nu/\omega}$ under the (generally satisfied)

104 assumption $k\delta_\nu \ll 1$. Consequently, we ignore viscous damping of waves as they prop-
 105 agate. In contrast, we must retain the Coriolis force since, as demonstrated by Hassel-
 106 mann (1970), $O(f/\omega)$ corrections put horizontal and vertical velocity components out
 107 of quadrature, with impact on the wave-averaged dynamics.

Integrating the $O(\alpha^2)$ equations over a wave period, we obtain the wave-averaged
 mean flow equations (e.g. Huang, 1979)

$$\partial_t \bar{u} - f v_L = -\partial_x \bar{p} + \nu \nabla^2 \bar{u}, \quad \partial_t \bar{v} + f u_L = -\partial_y \bar{p} + \nu \nabla^2 \bar{v}, \quad (2a)$$

$$\partial_t \bar{w} = -\partial_z \bar{p} + \nu \nabla^2 \bar{w}, \quad \partial_x \bar{u} + \partial_y \bar{v} = -\partial_z \bar{w}, \quad (2b)$$

108 where the overbar denotes a time average, $\mathbf{u}_L = \bar{\mathbf{u}} + \mathbf{u}_s$ is the Lagrangian (or particle-
 109 transport) velocity, with $\bar{\mathbf{u}} = \overline{\mathbf{u}_2}$ the Eulerian-mean velocity and \mathbf{u}_s the Stokes drift,
 110 and the horizontal component of the Coriolis vector introduces only higher-order cor-
 111 rections to the flow. Without the shear and pressure terms, equations (2a) and (2b) cor-
 112 respond to those considered by Hasselmann (1970). The Coriolis terms include the Coriolis-
 113 Stokes forcing $-f \hat{z} \times \mathbf{u}_s$ (Hasselmann, 1970; Polton et al., 2005), which drives an Eu-
 114 lerian ‘anti-Stokes flow’, cancelling the Stokes drift and exciting inertial oscillations, and
 115 explains Ursell (1950)’s prediction of zero net drift for periodic waves in a rotating frame.

We focus on the horizontal momentum equations (2a) in the Stokes layer, that is,
 the top $O(k^{-1})$ -deep layer of the ocean where the Stokes drift and hence the Coriolis-
 Stokes forcing are localised. One of the boundary conditions is provided by averaging
 the condition of zero tangential stress in (1b) (Longuet-Higgins (1953), Ünlüata & Mei
 (1970), Xu & Bowen (1994) and Seshasayanan & Gallet (2019)); it is given by

$$\partial_z \bar{\mathbf{u}}_H|_{z=0} = \partial_z \mathbf{u}_{sH}|_{z=0}. \quad (3)$$

116 Examining the viscous but non-rotating case, Longuet-Higgins (1953) originally showed
 117 that vorticity is transported from the viscous boundary layers into the fluid interior, af-
 118 fecting the mass transport profile (Ünlüata & Mei, 1970; Xu & Bowen, 1994; Seshasayanan
 119 & Gallet, 2019). Additional Eulerian-mean wave-induced transport, known as boundary-
 120 layer streaming, occurs in the boundary layer (e.g. (Grue & Kolaas, 2017)). The con-
 121 tributions of Hasselmann (1970) and Longuet-Higgins (1953) (and the theory of wind-
 122 driven currents of Ekman (1905)) were unified by Xu & Bowen (1994) into a model of
 123 wave (and wind-) driven flow in finite-depth water.

In the Stokes layer, vertical gradients dominate over horizontal ones. It follows from
 (2b) that the vertical velocity component can be neglected and hence p is z -independent.
 Introducing the complex notation $\mathcal{U} = \bar{u} + i\bar{v}$ as in Huang (1979), we obtain the Ekman-
 Stokes equations

$$(\partial_t + if - \nu \partial_z^2) \mathcal{U} = -if \mathcal{U}_s(\mathbf{x}, z, t), \quad \partial_z \mathcal{U} = \partial_z \mathcal{U}_s(\mathbf{x}, z, t) \Big|_{z=0}, \quad \lim_{z \rightarrow -\infty} \mathcal{U} = 0, \quad (4a,b,c)$$

124 where the two boundary conditions follow from (3) and the requirement that the solu-
 125 tion can be matched to a weak Eulerian flow outside the Stokes layer. The Eulerian Ekman-
 126 Stokes velocity solving (4) is driven by the Stokes drift in two ways, via the Coriolis-Stokes
 127 forcing in the fluid interior (Polton et al., 2005) and via the wave stress condition (4b).

128 Note that a surface wind stress could be added to the boundary condition (4b); by
 129 linearity, the wind-driven Ekman velocity would simply be superimposed in convolution
 130 form on the wave-driven velocity we obtain (for example, Madsen (1978) Eq. (21) for linearly-
 131 varying $\nu(z)$). Assuming the wind stress is greater than the wave stress so that the lat-
 132 ter can be omitted, Lewis & Belcher (2004) derive solutions to (4) for non-constant vis-
 133 cosity, but do not account for time-dependence of the wave-induced Eulerian response
 134 arising from the time-variation of the surface wave field and the associated Stokes drift.

2.2 Solution by Laplace transform

We solve (4) by Laplace transform, assuming that the Stokes drift \mathcal{U}_s has a time-independent vertical structure $\exp(2kz)$, corresponding to a quasi-monochromatic wave field, but an otherwise arbitrary time dependence. Denoting the Laplace transform by a tilde, with

$$\tilde{g}(s) = \mathcal{L}\{g(t)\} = \int_0^\infty g(t)e^{-st}dt, \quad \tilde{g}(s) = \mathcal{L}^{-1}\{\tilde{g}(s)\} = \frac{1}{2\pi i} \int_{\gamma-i\infty}^{\gamma+i\infty} \tilde{g}(s)e^{st}ds, \quad (5a,b)$$

where γ is a real number such that the contour path of integration is in the region of convergence of $\tilde{g}(s)$, we find

$$\tilde{\mathcal{U}} = 2k \left(1 + \frac{if}{s+if-4k^2\nu} \right) \frac{\tilde{\mathcal{U}}_s e^{z\sqrt{(s+if)/\nu}}}{\sqrt{(s+if)/\nu}} - \frac{if\tilde{\mathcal{U}}_s e^{2kz}}{s+if-4k^2\nu}. \quad (6)$$

This is the sum of a particular solution – the second term – which can be interpreted as a partial anti-Stokes flow, varying over the Stokes depth $\delta_s = (2k)^{-1}$, and a homogeneous solution – the first term – varying over the Ekman depth $\delta_E = \sqrt{2\nu/f}$, which includes a contribution driven by the vertical shear of the Stokes drift through the boundary condition (4b) (second term in the brackets in (6)).

A special case of (6) occurs if \mathcal{U}_s approaches a steady value $\overline{\mathcal{U}}_s$ as $t \rightarrow \infty$. Then $\overline{\mathcal{U}}$ tends to the time-independent solution (e.g. Seshasayanan & Gallet (2019))

$$\overline{\mathcal{U}} = \frac{(1-i)D}{2} \overline{\mathcal{U}}_s \left(1 + \frac{1}{1+iD^2/2} \right) e^{(1+i)z/\delta_E} - \frac{\overline{\mathcal{U}}_s e^{2kz}}{1+iD^2/2}, \quad (7)$$

where $D \equiv \delta_E/\delta_s$ is the fixed ratio of Ekman to Stokes depths. In the limit $D \rightarrow 0^+$, equation (7) tends to $-\overline{\mathcal{U}}_s \exp(2kz)$: up to an inertial oscillation this is the so-called ‘anti-Stokes’ Eulerian-mean flow, predicted by Hasselmann (1970) to be induced by periodic waves in a rotating, inviscid ocean. Viscosity acts to reduce the shear in the anti-Stokes flow, so that a nonzero Lagrangian-mean velocity remains.

2.3 Ekman–Stokes kernel

We now use the Laplace convolution theorem to write the unsteady solution for the Ekman–Stokes mean flow as a function of time for arbitrary Stokes drift as

$$\mathcal{U}(\mathbf{x}, z, t) = \mathcal{U}_s|_{z=0} * K(z, t), \quad (8)$$

where $*$ denotes convolution in time and

$$K(z, t) = \mathcal{L}^{-1} \left\{ \frac{2ke^{z\sqrt{(s+if)/\nu}}}{\sqrt{(s+if)/\nu}} + \frac{if}{s+if-4k^2\nu} \left(\frac{2ke^{z\sqrt{(s+if)/\nu}}}{\sqrt{(s+if)/\nu}} - e^{2kz} \right) \right\}. \quad (9)$$

The convolution kernel $K(z, t)$, which we will term the Ekman–Stokes kernel, can be evaluated by deforming the integration contour involved in the inverse Laplace transform to obtain (see supplementary material)

$$K(z, t) = 2k\sqrt{\nu}e^{-ift} \frac{e^{-z^2/(4\nu t)}}{\sqrt{\pi t}} - ife^{(4k^2\nu-if)t} \sum_{\pm} \frac{e^{\pm 2kz}}{2} \operatorname{erfc} \left(\sqrt{4k^2\nu t} \pm \frac{z}{\sqrt{4\nu t}} \right), \quad (10)$$

where \sum_{\pm} denotes the sum of the plus and minus terms and we use the complementary error function $\operatorname{erfc}(x) = 1 - \operatorname{erf}(x)$. An equivalent form emphasising the dependence on wave parameters uses the scaled error function $\operatorname{erfcx}(t) = e^{t^2} \operatorname{erfc}(t)$ and reads

$$K(z, t) = 2k\sqrt{\nu}e^{-ift} \frac{e^{-z^2/(4\nu t)}}{\sqrt{\pi t}} - ife^{-ift} \frac{e^{-z^2/(4\nu t)}}{2} \sum_{\pm} \operatorname{erfcx} \left(\sqrt{4k^2\nu t} \pm \frac{z}{\sqrt{4\nu t}} \right). \quad (11)$$

Limit	Behaviour	Theory
$t \rightarrow \infty$	$2k\sqrt{\nu}e^{-ift}/\sqrt{\pi t} [1 - if/(4k^2\nu) (1 - (1 + 2k^2z^2)/(4k^2\nu t))]$	long-time limit
$t \rightarrow 0^+$	$8\nu k^2\delta(z/\delta_s) - ife^{2kz}$	short-time limit
$\nu \rightarrow 0^+$	$-ife^{-ift}e^{2kz}$	Hasselmann (1970)
$f \rightarrow 0^+$	$2k\sqrt{\nu}e^{-z^2/(4\nu t)}/\sqrt{\pi t}$	Longuet-Higgins (1953)

Table 1. Asymptotic behaviour of the Ekman–Stokes kernel $K(z, t)$.

147 The Ekman–Stokes kernel K captures the (Eulerian-mean) flow response to the Stokes
 148 drift. The $1/\sqrt{t}$ describes the establishment of an Ekman spiral driven by the wave-induced
 149 surface stress; the if terms describe the impact of the Coriolis–Stokes forcing. Note that
 150 the dimension of $K(z, t)$ is time^{-1} .

Several limits of the kernel are of interest; they are given in dimensional terms in
 Table 1. The limits $\nu \rightarrow 0^+$ and $f \rightarrow 0^+$ are best understood by rewriting (11) in terms
 of the dimensionless parameters $D = \delta_E/\delta_s$, $\zeta = 2kz$ and $\tau = ft$ to obtain

$$K(\zeta, \tau)/f = De^{-i\tau} \frac{e^{-\zeta^2/(2D^2\tau)}}{\sqrt{2\pi\tau}} - \frac{i}{2} \sum_{\pm} e^{-i\tau - \zeta^2/(2D^2\tau)} \operatorname{erfcx} \left(D\sqrt{\frac{\tau}{2}} \pm \frac{\zeta}{\sqrt{2D^2\tau}} \right). \quad (12)$$

151 When $D \gg 1$, e.g. because $f \rightarrow 0^+$, the Coriolis–Stokes sum term in (12) is negligi-
 152 ble and the flow becomes the Longuet-Higgins (1953) response to the wave stress at the
 153 surface. In contrast, for $D \ll 1$, e.g. as $\nu \rightarrow 0^+$, the anti-Stokes result of Hasselmann
 154 (1970) is approached but non-uniformly in ζ . This singular behaviour arises since for any
 155 nonzero D the shear condition at the surface cannot be met by an exact anti-Stokes flow,
 156 resulting in a thin layer of depth $\sim \sqrt{\nu/f}$ near the surface where cancellation of the Stokes
 157 drift is imperfect (e.g. Seshasayanan & Gallet (2019)). Over long times $\tau \rightarrow \infty$, the
 158 Coriolis–Stokes terms decay on the viscous rather than the inertial timescale, despite ow-
 159 ing their existence to Earth’s rotation.

160 The magnitude and argument of the dimensionless kernel $K(\zeta, \tau)$ are shown in Fig-
 161 ure 1 for $D = 1$. The magnitude is largest towards $(\tau, \zeta) = (0, 0)$ due to the singular
 162 behaviour discussed above. The kernel has the character of an amplitude-decaying in-
 163 ertial oscillation with period $2\pi/f$ with an orientation in the horizontal plane that os-
 164 cillates with the inertial period. Equation (11) together with the convolution in time (8)
 165 is the key result of this letter. Taking as inputs a time series of Stokes drift and estimates
 166 of the peak wavenumber k , Coriolis parameter f and turbulent viscosity ν , these equa-
 167 tions produce a time series of the associated (Eulerian-mean) Ekman–Stokes current at
 168 any vertical elevation z , which can simply be added to the time series of the Stokes drift
 169 to give the Lagrangian-mean current relevant for marine litter transport. An open-source
 170 implementation in Python is provided as supplementary material.

171 3 Sample calculations of the Ekman–Stokes flow

172 3.1 Idealised storm

173 To demonstrate the use of the Ekman–Stokes kernel, we calculate the Eulerian re-
 174 sponse to a Gaussian Stokes drift profile lasting approximately 24 hours to represent an
 175 idealised storm. Specifically, we set $u_s(z = 0) = u_s^* \exp(-(t - t^*)^2/(\sigma^2))$ (and $v_s = 0$)
 176 with $\sigma = 6$ hrs and magnitude $u_s^* = 0.070$ m/s being reached at $t^* = 24$ hrs. Choos-
 177 ing $f = 1.0 \times 10^{-4}$ s $^{-1}$ and $\nu = 1.0 \times 10^{-2}$ m 2 s $^{-1}$ ($D = 1.1$), we set $\mathcal{U}(z = 0, t = 0) =$
 178 0 and evaluate the response for 1 week.

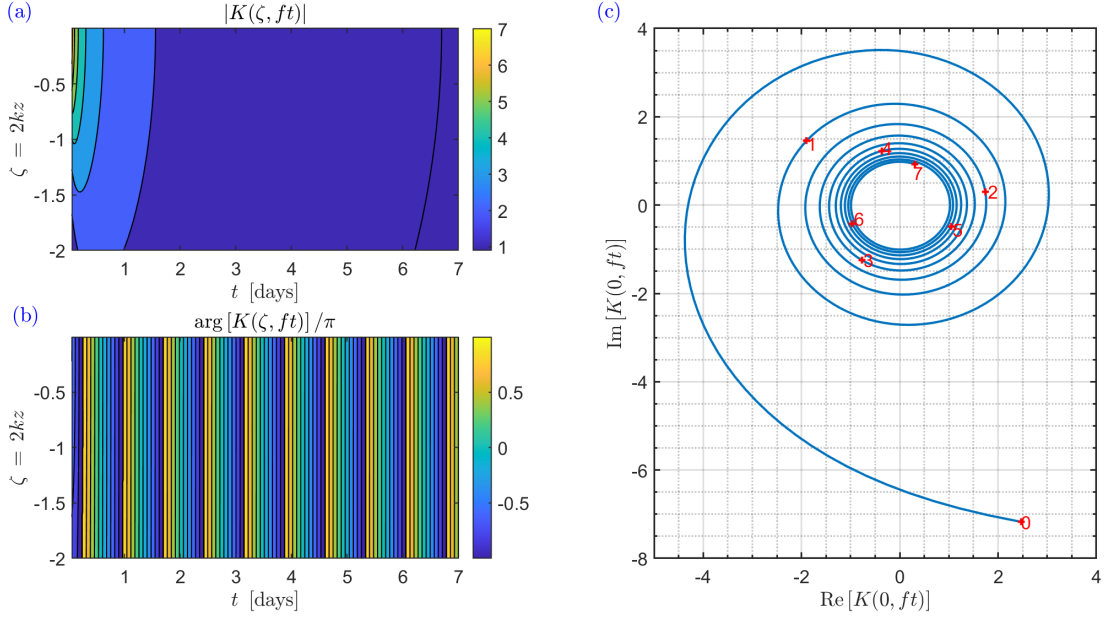


Figure 1. Ekman–Stokes kernel $K(\zeta, \tau)$ for $D = 1$ (with $f = 1 \times 10^{-4} \text{s}^{-1}$): (a) magnitude and (b) argument as a function of depth and time, and (c) hodograph at the surface ($\zeta = 0$) with time (in days) shown in red. In panel (a) we have saturated the colour scale, as the kernel is singular at $(\zeta, \tau) = (0, 0)$.

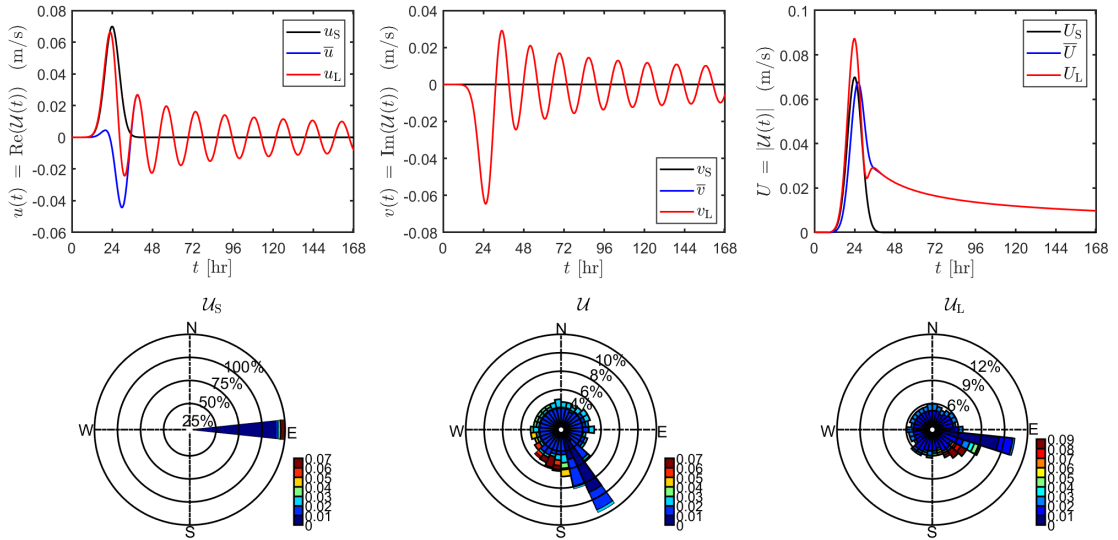


Figure 2. Top: Time series of wave-induced velocities formed in response to an idealised 24-hr Gaussian storm in the Northern Hemisphere showing the two components and magnitude of the Stokes drift U_s (black), Eulerian-mean velocity U (blue) and Lagrangian velocity U_L (red). **Bottom:** Wave roses for U_s , U , and U_L , with radial distance representing the fraction of time during which the velocity has a given direction, and colour indicating magnitude in m/s.

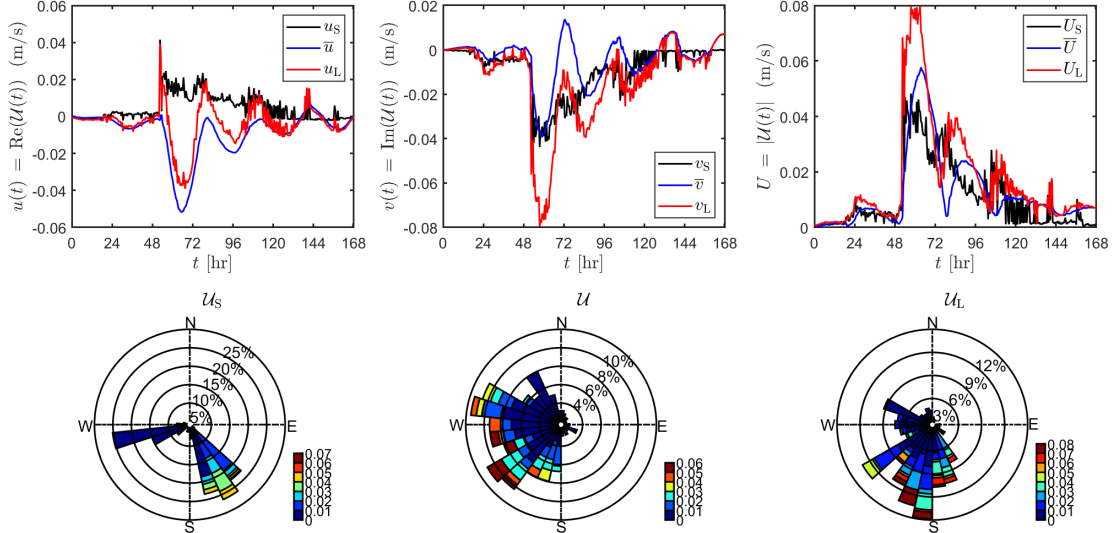


Figure 3. **Top:** Time series (14/05/00 15:41 – 22/05/00 09:41 UTC) of wave-induced velocities computed from buoy data from San Nicolas Island (33.22° N, 119.88° W), with colours as in Fig. 2. **Bottom:** Corresponding wave roses, as in Fig. 2.

179 In figure 2 we plot the u and v components and magnitudes, respectively, of the
 180 second-order currents over a week-long period. The sum of Stokes drift (black) and Ekman–
 181 Stokes flow (blue) gives the Lagrangian (transport) velocity (red). Beneath, wave roses
 182 are plotted for these second-order currents. The angular direction corresponds to the an-
 183 gular direction of propagation of the current (separated into 30 bins), the radius of each bar repre-
 184 sents the percentage of time during which the velocity has a given direction, and the colour
 185 scale divides the data into velocity amplitude ranges. Fig. 2 shows that the Stokes drift
 186 is reduced by a (delayed) partial ‘anti-Stokes’ flow in the opposing direction, a transverse
 187 component arises on the same time scale, and damped inertial oscillations are formed
 188 which remain after the storm has ceased. The resulting Lagrangian current is deflected
 189 by the large transverse component of the Ekman-Stokes flow, to the right in the North-
 190 ern Hemisphere (and to the left in the Southern Hemisphere).)

191 3.2 Buoy data

We use half-hourly records for the San Nicolas Island buoy (33.22° N, 119.88° W) obtained from CDIP (the Coastal Data Information Project) and estimate the Stokes drift using the formula

$$192 \mathcal{U}_s = g^{-1} \omega_p^3 A_p^2 \exp(2\bar{k}z) \exp(i\theta_p), \text{ where } A_p = H_s/4. \quad (13)$$

193 where θ_p is the peak wave direction, H_s is the significant wave height, and ω_p is the peak
 194 frequency calculated from the peak period T_p . By making a quasi-monochromatic ap-
 195 proximation, we assume the wavenumber spectrum is peaked about $k = \text{mean}(k_p) =$
 196 $\text{mean}(\omega_p^2/g)$, to leading order. We integrate (11) using the Stokes drift (13) by a trape-
 197 zoidal rule with time-step equal to the buoy sampling time. We define the surface value
 198 of the kernel as $\lim_{z \rightarrow 0^-} K(z, t)$ instead of directly setting $z = 0$, so that the singular
 behaviour at $(0, 0)$ is avoided.

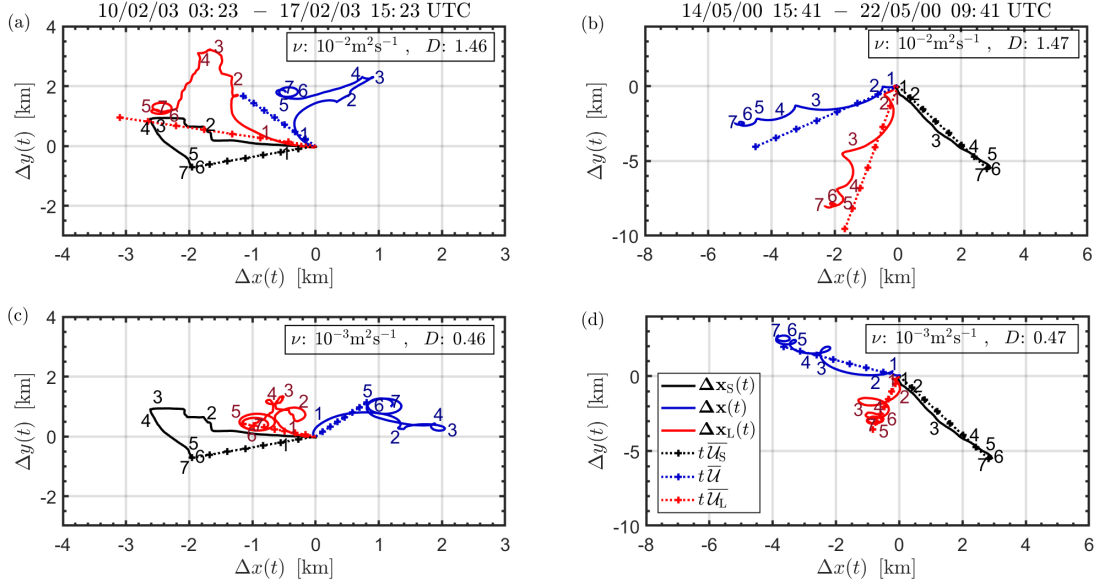


Figure 4. Particle paths at the surface ($z=0$) computed for the San Nicolas Island buoy using our Ekman–Stokes convolution kernel. **Columns:** two different time samples. **Rows:** different values of turbulent viscosity. The paths shown are obtained using the Stokes drift (black), Eulerian-mean velocity (blue) and Lagrangian-mean velocities (red). The dashed lines ignore time dependence of the Stokes drift and show the response to the average of the Stokes drift over the periods considered. All paths begin at $(\Delta x, \Delta y) = (0, 0)$. Numbers beside each line denote the number of days elapsed.

199 As in figure 2, the top panels of figure 3 show the u and v components and mag-
 200 nitudes of the second-order currents. The largest Stokes drift at San Nicolas Island over
 201 this time period is in a South-Southeasterly direction, though a share of very small val-
 202 ues arising from small-amplitude waves are also seen to propagate West-Southwest (cf.
 203 bottom-left panel, figure 3). In contrast, the Ekman–Stokes contribution is much more
 204 directionally-spread at all velocity amplitudes due to excited inertial oscillations. Super-
 205 imposing the two flows leads to a directionally-spread Lagrangian drift which veers to
 206 the right of the Stokes drift.

207 To find the displacement associated with the unsteady flows, we simplify the prob-
 208 lem by taking the wavenumber and Stokes drift time series to be uniform in space, which
 209 is valid for the relatively small accumulated displacements considered. Particle displac-
 210 ements are computed by time integrating the velocities obtained from our Ekman–Stokes
 211 kernel and are plotted in figure 4. Panels (a) and (c) show displacements over one week
 212 in February 2003 and (b) and (d) over a week in May 2000, with (b) corresponding to
 213 velocities plotted in figure 3. Line colours are consistent with figures 2 and 3. Straight
 214 dotted lines represent steady solutions i.e. (7) multiplied by time elapsed, with $\overline{U}_s =$
 215 mean(U_s). Evidently, the steady approximation causes errors in the prediction of net
 216 particle displacement. Instead of simply following the black trajectory being transported
 217 by the Stokes drift alone, we predict the particle will follow the red trajectory, being trans-
 218 ported by the Lagrangian velocity, the sum of the Stokes drift and the wave-induced Ekman–
 219 Stokes flow. For both time samples, the Lagrangian displacement is to the right of the
 220 displacement by the Stokes drift, as for the velocities. In the Southern Hemisphere, it
 221 will lie to the left of the Stokes drift.

222 We anticipate that the realistic range for viscosity is $O(10^{-3})$ - $O(10^{-2})$ m^2s^{-1} , es-
 223 timated from the vertical mixing coefficient $S_M = 0.30$ in Mellor & Blumberg (2004)
 224 by using the law of the wall. Comparing (c) and (d) with (a) and (b), the particle dis-
 225 placement is reduced and inertial oscillations are more pronounced for the smaller vis-
 226 cosity $\nu = 10^{-3}\text{m}^2\text{s}^{-1}$ in (c) and (d), since the directly opposing anti-Stokes flow in-
 227 creases in magnitude as viscosity decreases. For both values of ν (and values between
 228 them) the displacement is significantly altered in both magnitude and direction when
 229 the Ekman–Stokes flow is included.

230 4 Discussion and conclusions

231 Our analysis has demonstrated the need to add a so-called Ekman–Stokes flow to
 232 the Stokes drift to properly estimate the wave-induced Lagrangian-mean flow which trans-
 233 ports floating marine litter. We have derived an Ekman–Stokes convolution kernel which
 234 can readily be used to predict the wave-induced Eulerian-mean flow in the turbulent upper-
 235 ocean boundary layer on a rotating Earth. It incorporates three important effects: the
 236 surface wave stress, the Coriolis–Stokes forcing, and unsteadiness of the forcing and re-
 237 sponse.

238 We properly account for the wave stress at the surface. This is often neglected (e.g.
 239 Lewis & Belcher (2004); Polton et al. (2005); Onink et al. (2019)), though it may be of
 240 the same magnitude as the wind stress (Seshasayanan & Gallet, 2019). Including the wave
 241 stress will yield more accurate predictions of the Lagrangian drift, particularly when wind
 242 and waves are misaligned. Our model also incorporates the Coriolis–Stokes forcing which
 243 induces a partial anti-Stokes flow and alters the response over the Ekman depth $\delta_E =$
 244 $\sqrt{2\nu/f}$ (cf. Polton et al. (2005)). Our results demonstrate that for realistic values of eddy
 245 viscosity of 10^{-3} - 10^{-2} m^2s^{-1} there is only partial cancellation of the Stokes drift by an
 246 anti-Stokes flow. Perhaps most importantly, our approach shows that unsteadiness of the
 247 Stokes drift and the induced Eulerian response can be readily incorporated into mod-
 248 els of Lagrangian drift using a simple convolution. As passage times of storms are typ-
 249 ically $O(1/f)$, time variability of the problem is crucial for accurate predictions of drift.

250 Future work should improve our model in the following ways. For simplicity we have
 251 assumed a constant eddy viscosity, although our Ekman–Stokes kernel could be adapted
 252 for linearly-increasing eddy viscosity (Madsen (1977), Lewis & Belcher (2004)), which
 253 provides a more accurate representation of turbulence in the upper-ocean boundary layer.
 254 Additionally, Shrira & Almelah (2020) have presented a solution method accounting for
 255 time-dependence of the eddy viscosity due to processes such as mixed-layer restratifica-
 256 tion or wave breaking (Price & Sundermeyer, 1999). Parametrisations of turbulent vis-
 257 cosity should thus account for both time and depth variation.

258 In real oceans, wave spectra are broad-banded, leading to a more strongly sheared
 259 but depth-persistent Stokes drift than for a monochromatic spectrum (Webb & Fox-Kemper,
 260 2011). When complete information about the wave spectrum is available, the Ekman–
 261 Stokes kernel can be used to evaluate the contribution of each wavenumber to the Eulerian-
 262 mean velocity, which can then be summed to obtain a complete response. However, shear
 263 of the Stokes drift for realistic broad-banded spectra can be approximated using a monochro-
 264 matic profile with a modified depth dependence (see e.g. Breivik et al. (2014)). Alter-
 265 native Stokes drift depth-profiles would result in a different wave stress and functional
 266 form of the Coriolis–Stokes term in our Ekman–Stokes kernel.

267 Finally, we note that Seshasayanan & Gallet (2019) have recently shown that the
 268 steady Ekman–Stokes spiral is unstable to perturbations. Future work should consider
 269 the importance of this instability in the real ocean and how it might interact with un-
 270 steadiness of the Stokes drift.

271 **Acknowledgments**

272 T.S.v.d.B. was supported by a Royal Academy of Engineering Research Fellowship,
 273 J.V. by the UK Natural Environment Research Council grant NE/R006652/1. The au-
 274 thors thank Harry Cunningham for assistance writing the Python script in the supple-
 275 mentary material. Buoy data was obtained from CDIP (Coastal Data Information Project)
 276 historical records (<https://cdip.ucsd.edu/>). The authors are grateful to Ø. Breivik for
 277 advice how to obtain representative values of viscosity.

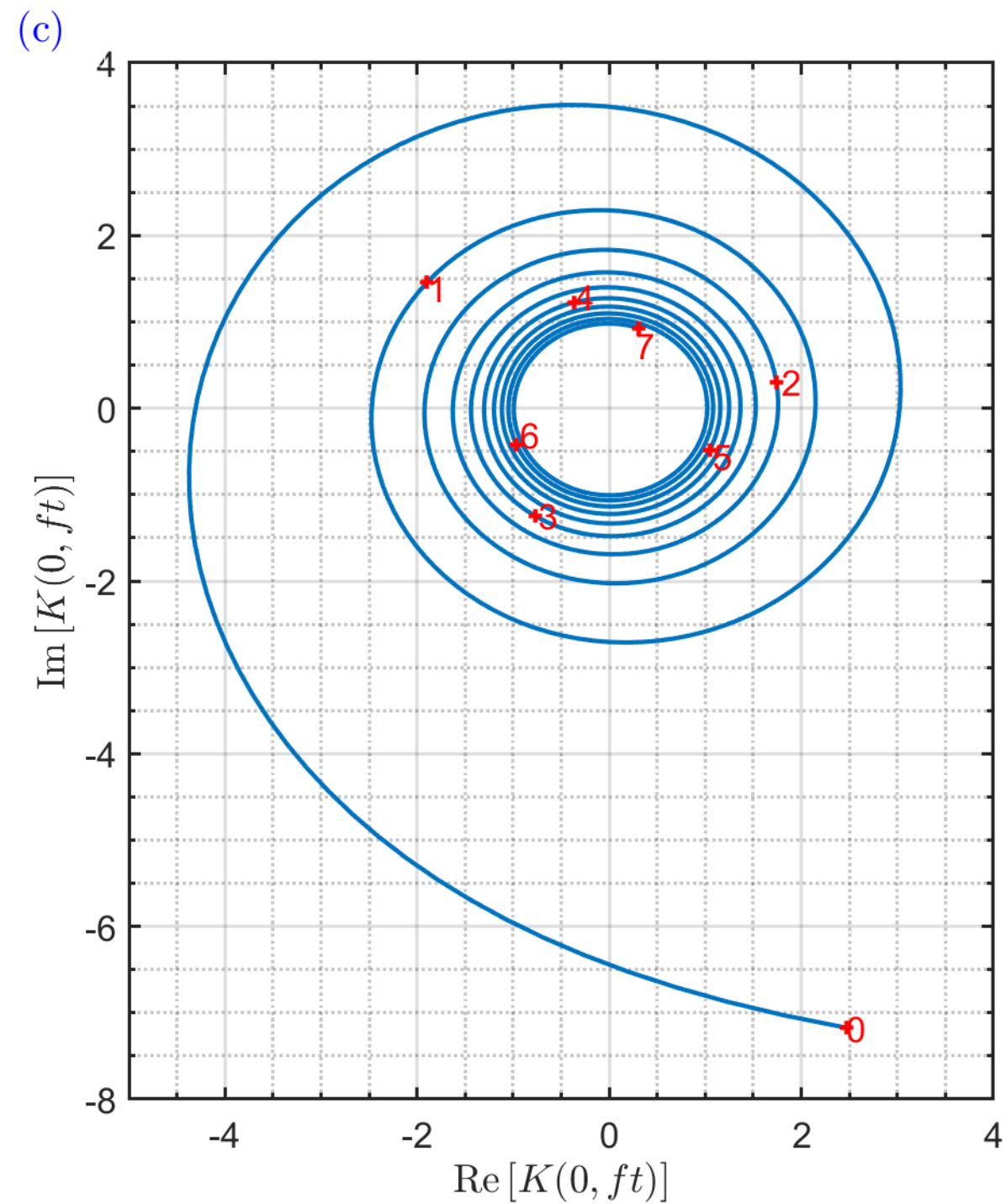
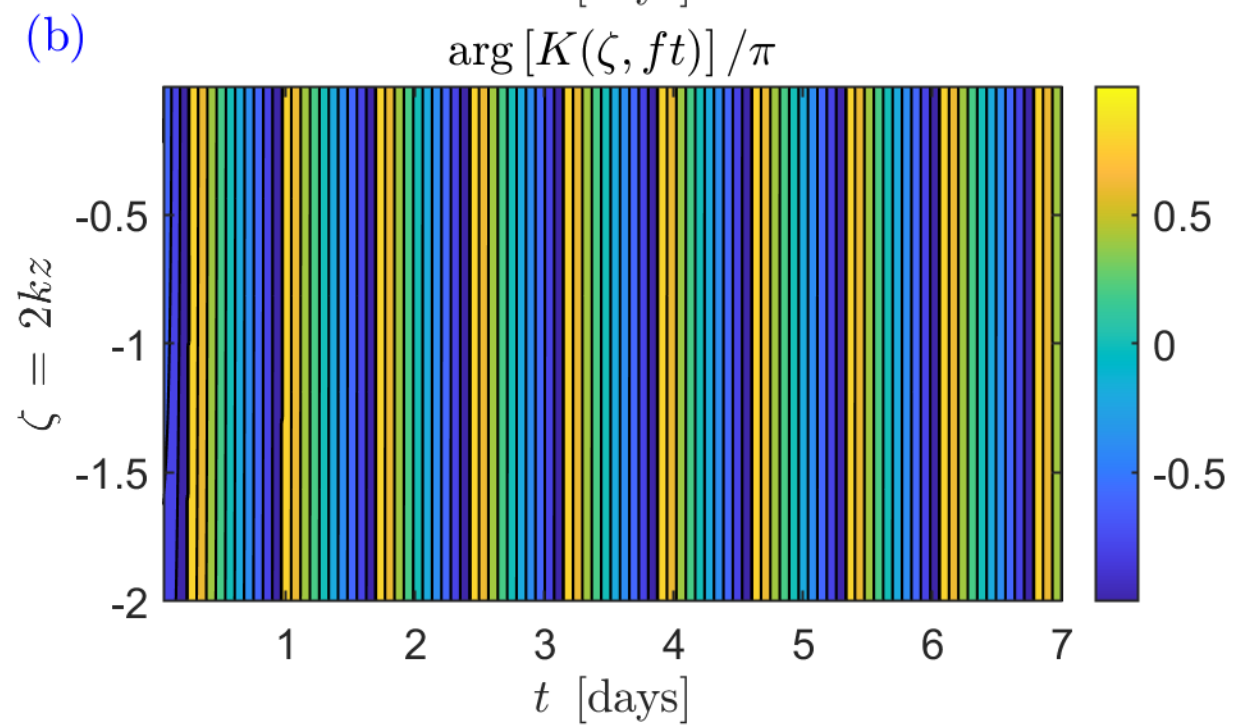
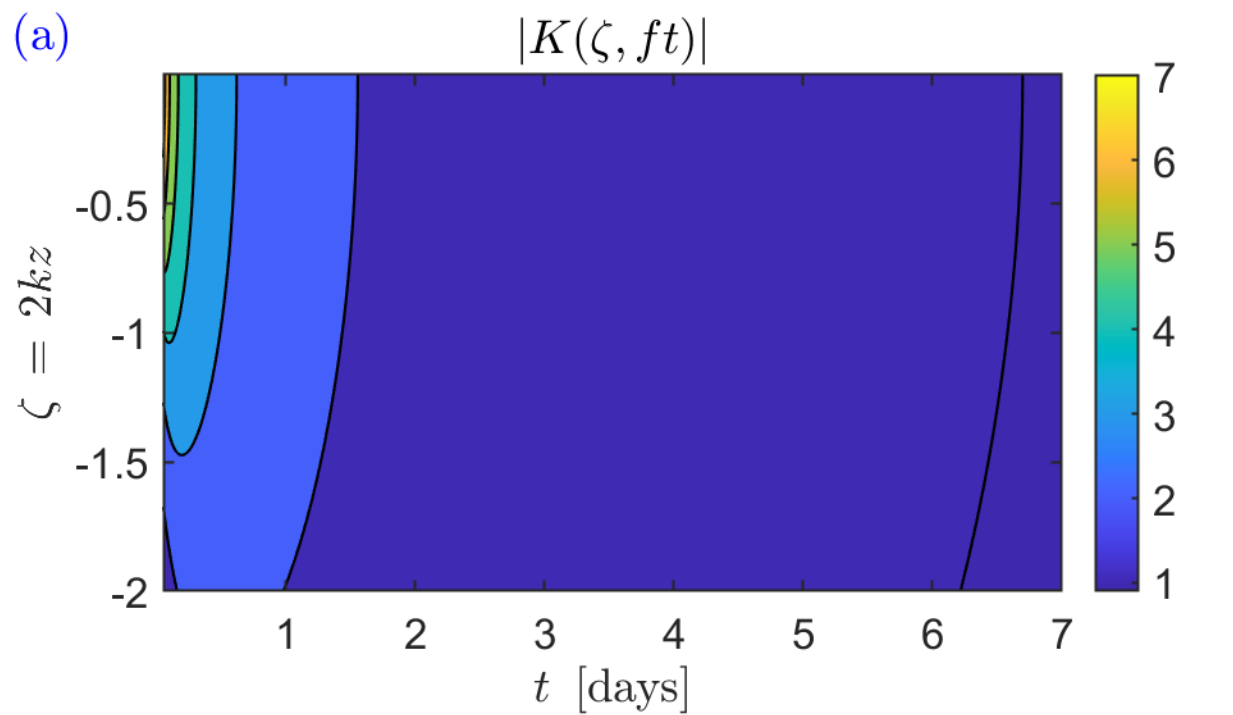
278 **References**

- 279 Andrady, A. L. (2011). Microplastics in the marine environment. *Mar. Pollut. Bull.*,
 280 *62*(8), 1596-1605. doi: 10.1016/j.marpolbul.2011.05.030
- 281 Breivik, Ø., Janssen, P., & Bidlot, J.-R. (2014). Approximate Stokes drift profiles in
 282 deep water. *J. Phys. Oceanogr.*, *44*(9), 2433-2445. doi: 10.1175/JPO-D-14-0020.1
- 283 Breivik, Ø., Mogensén, K., Bidlot, J.-R., Balmaseda, M. A., & Janssen, P. (2015).
 284 Surface wave effects in the NEMO ocean model: Forced and coupled experiments.
 285 *J. Geophys. Res.: Oceans*, *120*(4), 2973-2992. doi: 10.1002/2014JC010565
- 286 Bühler, O. (2014). *Waves and mean flows* (2nd ed.). Cambridge University Press,
 287 Cambridge, UK.
- 288 Cózar, A., Echevarría, F., González-Gordillo, J. I., Irigoien, X., Úbeda, M.,
 289 Hernández-León, S., ... Duarte, C. M. (2014). Plastic debris in the open ocean.
 290 *Science*, *111*(28), 10239-10244. doi: 10.1073/pnas.1314705111
- 291 Delandmeter, P., & van Sebille, E. (2019). The parcels v2.0 Lagrangian framework:
 292 new field interpolation schemes. *Geosci. Model Dev.*, *12*(8), 3571-3584. doi: 10
 293 .5194/gmd-12-3571-2019
- 294 Dobler, D., Huck, T., Maes, C., Grima, N., Blanke, B., Martinez, E., & Arduin,
 295 F. (2019). Large impact of Stokes drift on the fate of surface floating de-
 296 bris in the South Indian Basin. *Marine Pollution Bulletin*, *148*, 202-209. doi:
 297 doi.org/10.1016/j.marpolbul.2019.07.057
- 298 Ekman, V. W. (1905). On the influence of the Earth's rotation on ocean-currents.
 299 *Ark. Mat. Astron. Fys.*, *2*(11), 1-53.
- 300 Eriksen, M., Lebreton, L. C. M., Carson, H. S., Thiel, M., Moore, C. J., Borerro,
 301 J. C., ... Reisser, J. (2014). Plastic pollution in the world's oceans: More than 5
 302 trillion plastic pieces weighing over 250,000 tons afloat at sea. *PLoS ONE*, *9*(12),
 303 e111913. doi: 10.1371/journal.pone.0111913
- 304 Fraser, C., Morrison, A., Hogg, A. M., Macaya, E., van Sebille, E., Ryan, P.,
 305 ... Waters, J. (2018). Antarctica's ecological isolation will be broken by
 306 storm-driven dispersal and warming. *Nature Climate Change*, *8*(8). doi:
 307 10.1038/s41558-018-0209-7
- 308 Geyer, R., Jambeck, J. R., & Lavender Law, K. (2017). Production, use, and fate of
 309 all plastics ever made. *Sci. Adv.*, *3*(7), e1700782. doi: 10.1126/sciadv.1700782
- 310 Goldstein, M. C., Rosenberg, M., & Cheng, L. (2012). Increased oceanic microplas-
 311 tic debris enhances oviposition in an endemic pelagic insect. *Biol. Lett.*, *8*, 817-20.
 312 doi: 10.1098/rsbl.2012.0298
- 313 Grue, J., & Kolaas, J. (2017). Experimental particle paths and drift velocity in steep
 314 waves at finite water depth. *J. Fluid Mech.*, *810*, R1. doi: 10.1017/jfm.2016.726
- 315 Hasselmann, K. (1970). Wave-driven inertial oscillations. *Geophys. Fluid Dyn.*, *1*,
 316 463-502. doi: 10.1080/03091927009365783
- 317 Huang, N. E. (1979). On surface drift currents in the ocean. *J. Fluid Mech.*, *91*(1),
 318 191-208. doi: 10.1017/S0022112079000112
- 319 Iwasaki, S., Isobe, A., Kako, S., Uchida, K., & Tokai, T. (2017). Fate of microplas-
 320 tics and mesoplastics carried by surface currents and wind waves: A numerical
 321 model approach in the Sea of Japan. *Marine Pollution Bulletin*, *121*(1), 85-96.

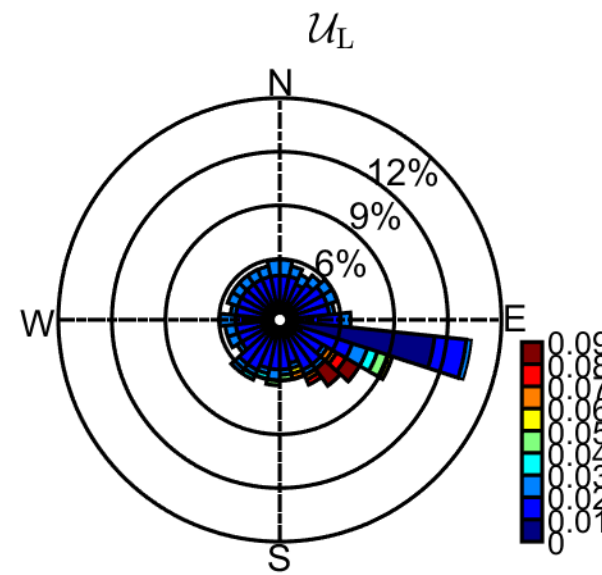
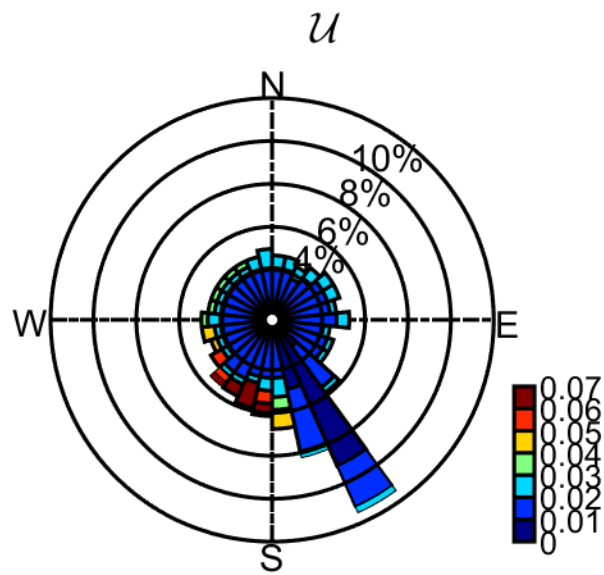
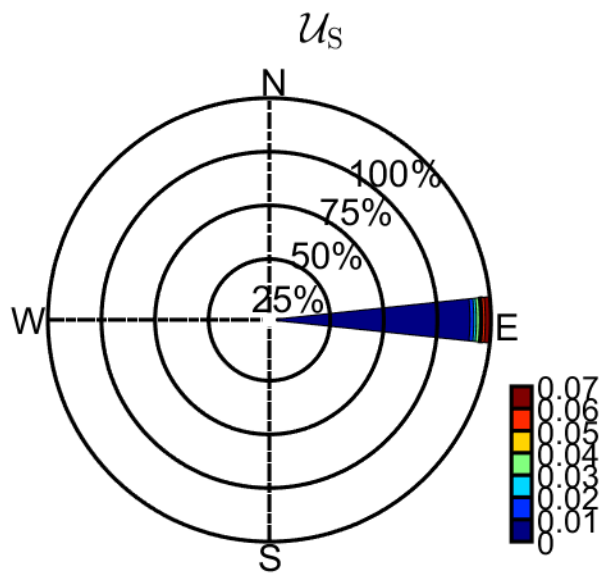
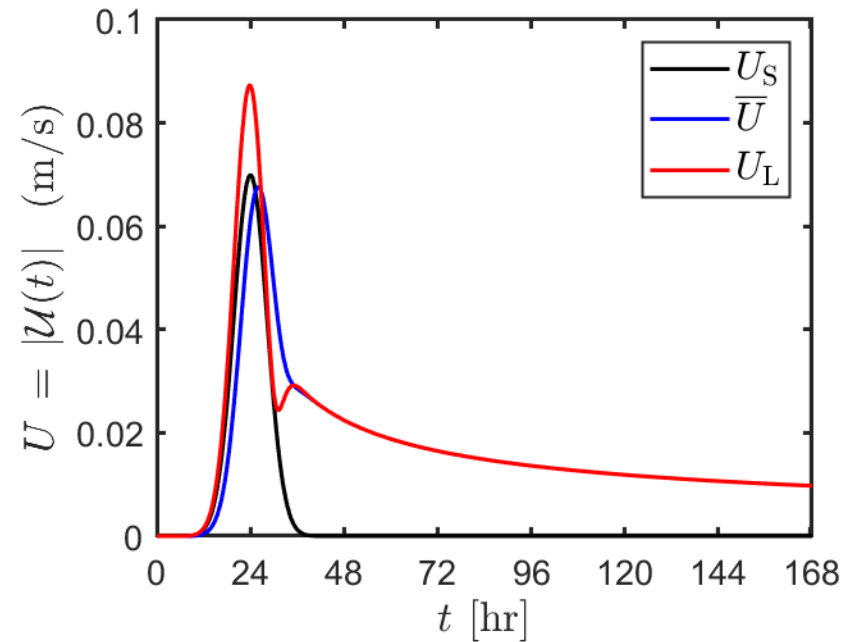
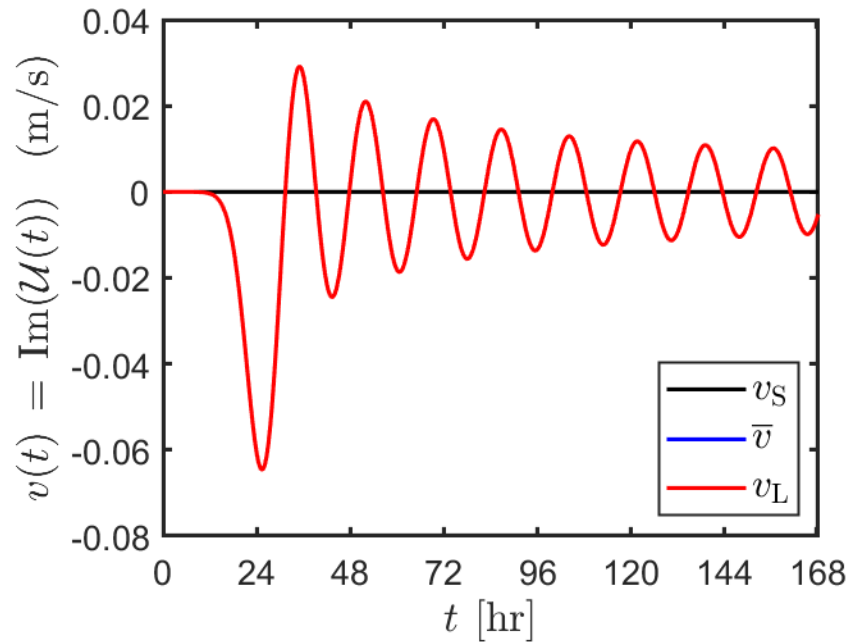
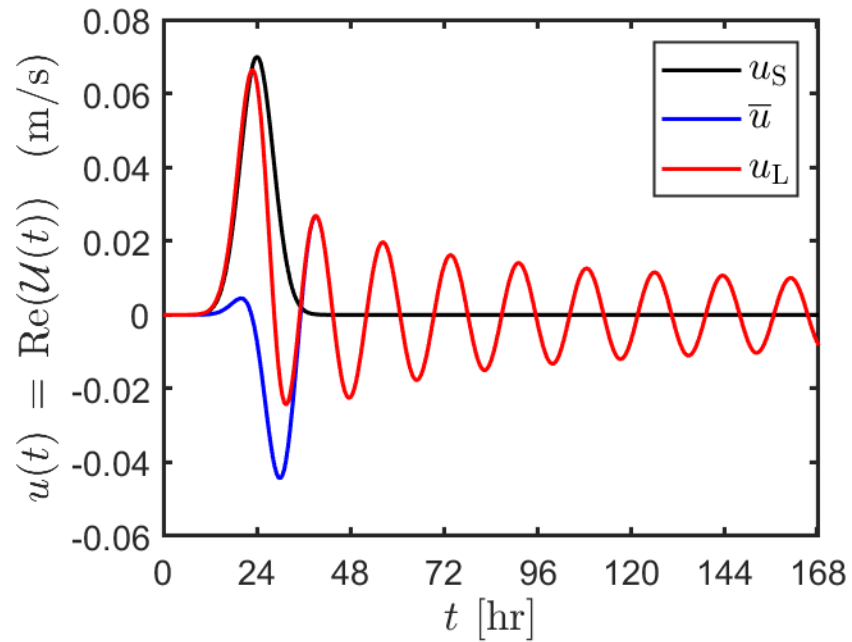
- doi: doi.org/10.1016/j.marpolbul.2017.05.057
- Jambeck, J. R., Geyer, R., Wilcox, C., Siegler, T. R., Perryman, M., Andrady, A.,
 . . . Lavender Law, K. (2015). Plastic waste inputs from land into the ocean.
Science, *347*(6223), 768-771. doi: 10.1126/science.1260352
- Lavender Law, K. (2017). Plastics in the marine environment. *Annu. Rev. Mar. Sci.*,
9, 205-229. doi: 10.1146/annurev-marine-010816-060409
- Lebreton, L., Egger, M., & Slat, B. (2019). A global mass budget for positively
 buoyant macroplastic debris in the ocean. *Sci. Rep.*, *9*, 12922. doi: 10.1038/s41598-
 019-49413-5
- Lewis, D., & Belcher, S. (2004). Time-dependent, coupled, Ekman boundary layer
 solutions incorporating Stokes drift. *Dynam. Atmosph. and Oceans*, *37*(4), 313-
 351. doi: doi.org/10.1016/j.dynatmoce.2003.11.001
- Longuet-Higgins, M. S. (1953). Mass transport in water waves. *Phil. Trans. Roy.
 Soc. London A*, *245*(903), 535-581. doi: 10.1098/rsta.1953.0006
- Madsen, O. S. (1977). A realistic model of the wind-induced Ekman boundary
 layer. *J. Phys. Oceanogr.*, *7*(2), 248-255. doi: 10.1175/1520-0485(1977)007<0248:
 ARMOTW>2.0.CO;2
- Madsen, O. S. (1978). Mass transport in deep-water waves. *J. Phys. Oceanogr.*,
8(6), 1009-1015. doi: 10.1175/1520-0485(1978)008<1009:MTIDWW>2.0.CO;2
- Mellor, G., & Blumberg, A. (2004). Wave breaking and ocean surface layer thermal
 response. *J. Phys. Oceanogr.*, *34*(3), 693-698. doi: 10.1175/2517.1
- Onink, V., Wichmann, D., Delandmeter, P., & van Sebille, E. (2019). The
 role of Ekman currents, geostrophy, and Stokes drift in the accumulation of
 floating microplastic. *J. Geophys. Res.: Oceans*, *124*(3), 1474-1490. doi:
 10.1029/2018JC014547
- Ostle, C., Thompson, R., Broughton, D., Gregory, L., Wootton, M., & Johns, D. G.
 (2019). The rise in ocean plastics evidenced from a 60-year time series. *Nat.
 Commun.*, *10*, 1622. doi: 10.1038/s41467-019-09506-1
- Polton, J., Lewis, D., & Belcher, S. (2005). The role of wave-induced Coriolis-Stokes
 forcing on the wind-driven mixed layer. *J. Phys. Oceanogr.*, *35*(4), 444-457. doi:
 10.1175/JPO2701.1
- Price, J. F., & Sundermeyer, M. A. (1999). Stratified Ekman layers. *J. Geophys.
 Res.: Oceans*, *104*(C9), 20467-20494. doi: 10.1029/1999JC900164
- Seshasayanan, K., & Gallet, B. (2019). Surface gravity waves propagating in a rotat-
 ing frame: The Ekman-Stokes instability. *Phys. Rev. Fluids*.
- Shrira, V. I., & Almelah, R. B. (2020). Upper-ocean Ekman current dynamics: a
 new perspective. *J. Fluid Mech.*, *887*, A24. doi: 10.1017/jfm.2019.1059
- Stokes, G. G. (1847). On the theory of oscillatory waves. *Trans. Cam. Phil. Soc.*, *8*,
 441-455.
- Tolman, H. L. (2009). User manual and system documentation of WAVEWATCH III
 TM version 3.14 Technical Note.
- Ünlüata, U., & Mei, C. C. (1970). Mass transport in water waves. *J. Geophys. Res.*,
75(36), 7611-7618. doi: 10.1029/JC075i036p07611
- Ursell, F. (1950). On the theoretical form of ocean swell on a rotating earth.
Mon. Not. Roy. Astron. Soc., Geophys. Suppl., *6*(s1), 1-8. doi: 10.1111/
 j.1365-246X.1950.tb02968.x
- van den Bremer, T. S., & Breivik, Ø. (2017). Stokes drift. *Phil. Trans. Roy. Soc.
 London A*, *376*(2111). doi: 10.1098/rsta.2017.0104
- van Sebille, E., Aliani, S., Law, K. L., Maximenko, N., Alsina, J., A. Bagaev,
 M. B., . . . Wichmann, D. (2020). The physical oceanography of the trans-
 port of floating marine debris. *Environ. Res. Lett.*, *15*(2), 023003. doi:
 10.1088/1748-9326/ab6d7d
- van Sebille, E., Wilcox, C., Lebreton, L., Maximenko, N., Hardesty, B. D., van
 Franeker, J. A., . . . Law, K. L. (2015). A global inventory of small floating plas-

- 376 tic debris. *Environ. Res. Lett.*, *10*(12), 124006. doi: 10.1088/1748-9326/10/12/
377 124006
- 378 Webb, A., & Fox-Kemper, B. (2011). Wave spectral moments and Stokes drift esti-
379 mation. *Ocean Modelling*, *40*(3), 273-288. doi: doi.org/10.1016/j.ocemod.2011.08
380 .007
- 381 Wilcox, C., Hardesty, B. D., & Law, K. L. (2020). Abundance of floating plastic par-
382 ticles is increasing in the western North Atlantic Ocean. *Envir. Sci. Tech.*, *54*(2),
383 790-796. doi: 10.1021/acs.est.9b04812
- 384 Xu, Z., & Bowen, A. (1994). Wave- and wind-driven flow in water of finite depth.
385 *J. Phys. Oceanogr.*, *24*(9), 1850-1866. doi: 10.1175/1520-0485(1994)024<1850:
386 WAWDFI>2.0.CO;2

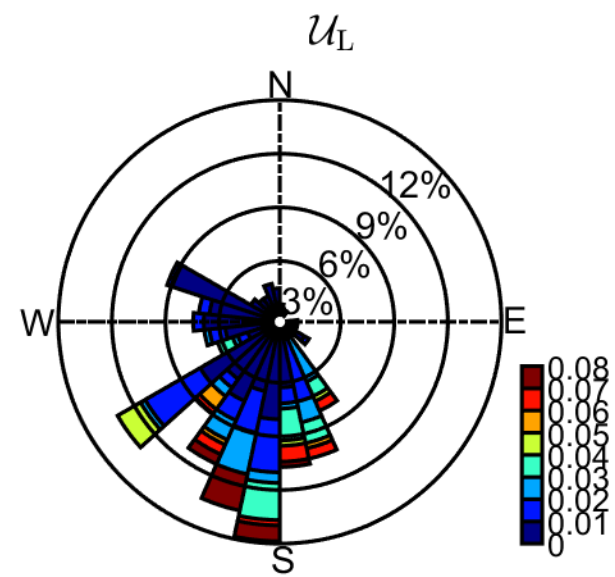
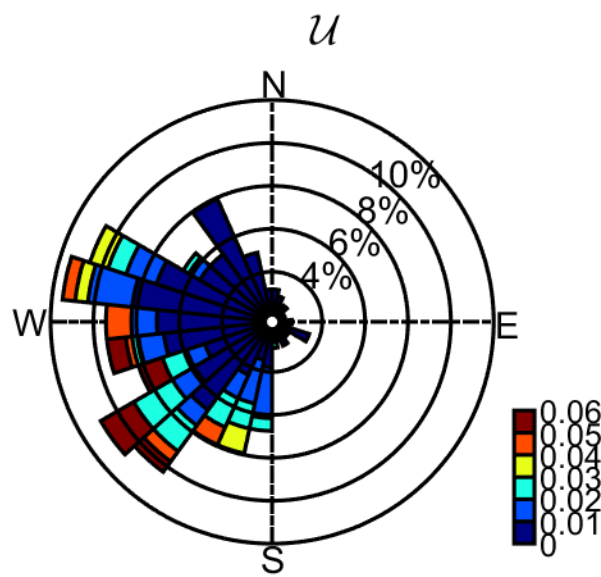
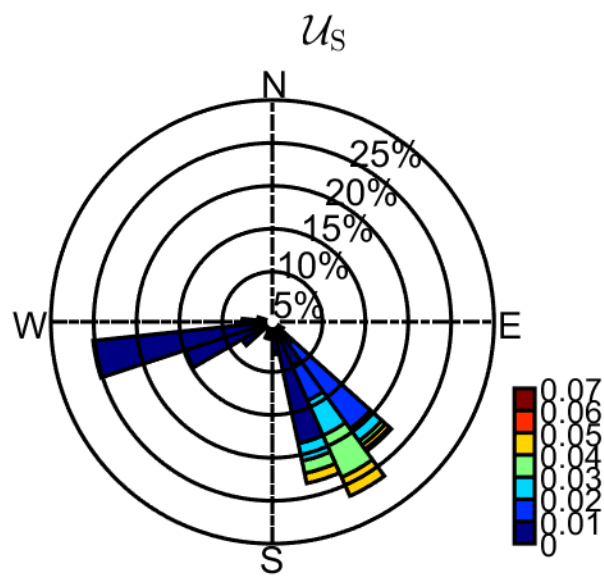
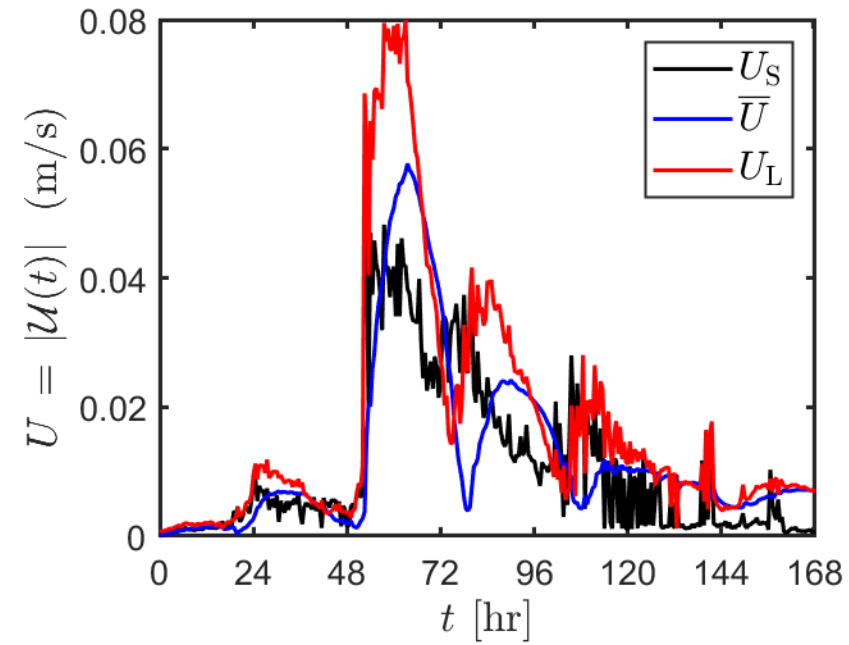
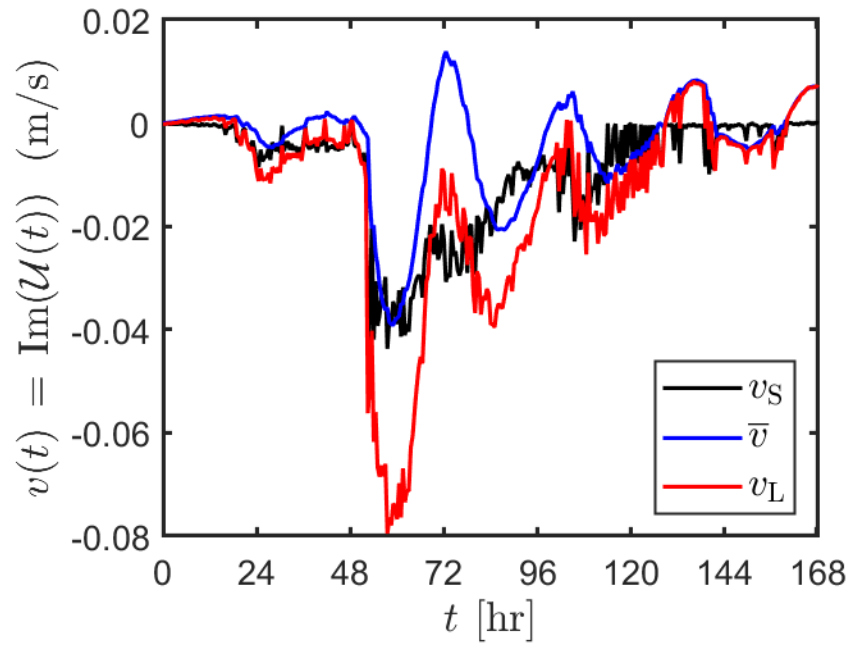
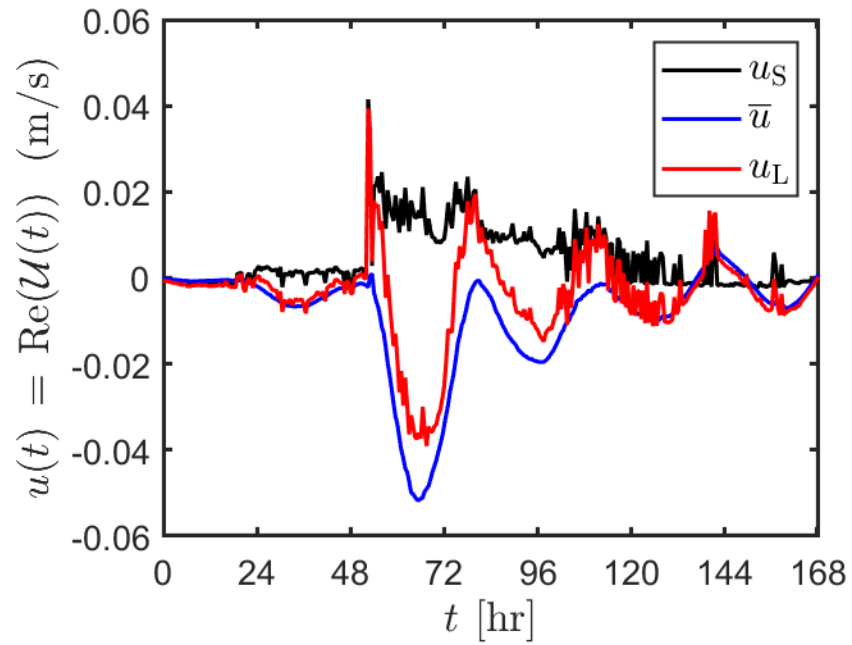
kernel_magarg.eps.



vel_gauss1.eps.



vel_r3_L.eps.



4fig_D_alt.eps.

